

Synthesis by picosecond laser ablation of ligand-free Ag and Au nanoparticles for SERS applications

Enza Fazio¹, Salvatore Spadaro¹, Marco Santoro¹, Sebastiano Trusso², Andrea Lucotti³, Matteo Tommasini³, Fortunato Neri¹, Paolo Maria Ossi^{4*}

¹ Dipartimento di Scienze Matematiche e Informatiche, Scienze Fisiche e Scienze della Terra (MIFT), Università di Messina, 98166 Messina, Italy

² CNR-Istituto per i Processi Chimico-Fisici, 98158 Faro Superiore, Messina, Italy

³ Dipartimento di Chimica, Materiali ed Ingegneria Chimica "G. Natta", Politecnico di Milano, Milano, Italy

⁴ Dipartimento Energia & Centre for NanoEngineered Materials and Surfaces -NEMAS, Politecnico di Milano, 20133 Milano, Italy

Abstract. The morphological and optical properties of noble metal nanoparticles prepared by picosecond laser generated plasmas in water were investigated. First, the ablation efficiency was maximized searching the optimal focusing conditions. The nanoparticle size, measured by Scanning Transmission Electron Microscopy, strongly depends on the laser fluence, keeping fixed the other deposition parameters such as the target to scanner objective distance and laser repetition frequency. STEM images indicate narrow gradients of NP sizes. Hence the optimization of ablation parameters favours a fine tuning of nanoparticles. UV-Visible spectroscopy helped to determine the appropriate laser wavelength to resonantly excite the localized surface plasmon to carry out Surface Enhanced Raman Scattering (SERS) measurements. The SERS activity of Ag and Au substrates, obtained spraying the colloids synthesized in water, was tested using crystal violet as a probe molecule. The good SERS performance, observed at excitation wavelength 785 nm, is attributed to aggregation phenomena of nanoparticles sprayed on the support.

1 Introduction

Over the last decade, noble metal nanoparticles (NPs) attracted strong interest due to their distinctive features that include their optically active plasmonic modes which originate intense absorption and scattering bands in the visible–near infrared interval; the extinction cross-section of NPs can be as high as 10^6 times that of the best organic chromophores and so is the local field amplification due to plasmon resonances at the basis of Surface Enhanced Raman Scattering (SERS); the easy surface functionalization with a broad range of organic molecules [1]. In particular, the use of noble metal nanostructures with plasmonic properties is rapidly spreading through biology and medicine [2]. In this respect, SERS technique is regarded as a promising analytical tool to analyse biological samples or drugs because it provides detailed spectroscopic information, which can be translated into imaging signal and adapted to an *in vivo* imaging system. A good basis for the intensity enhancement of SERS signals is a fine control of NP size, shape, spatial density and their distribution [3].

In the last few years, different preparation techniques have been used to prepare gold (Au) and silver (Ag) nanocolloids. However, wet chemical synthesis methods

(i.e. precipitation and sol-gel techniques) leave residual reagents which, unfortunately, cause the deactivation of NP surfaces. In contrast, pulsed laser ablation in liquid (PLAL) is a physico-chemical synthesis method that produces ligand-free, high purity NPs with superior conjugation efficiency, grafting density, electroaffinity toward charged biomolecules [4-6]. Nevertheless, with this synthesis method, it is difficult to achieve the large amounts of NPs required for industrial applications, in a short time, keeping unaltered the morphological properties. Being the ablation phenomenon in liquid a combination of different, probably competing, mechanisms in the laser–target–liquid system, it is of paramount importance to use an ultrafast laser source to minimize thermal effects and, then, to determine the appropriate ablation parameters to obtain NPs with tailored size distributions and concentration.

In this work, we investigate the morphological and optical properties of ligand-free Ag and Au NPs synthesized by picosecond (ps) laser ablation. First, we assessed the effects of the focusing conditions on the ablated spot diameter which, in turn, determines the operative fluence. Once established the optimal focusing conditions, we examined the effects of the ps pulsed-laser fluence to obtain an higher NPs productivity with a

* Corresponding author: paolo.ossi@polimi.it

fine tuning of NPs size, that is essential to prepare appropriate SERS active substrates.

2 Experimental

Pulsed laser ablation of high purity (99.9%) Ag and Au solid targets in deionized water (H₂O) was carried out using the second harmonic (532 nm) of a laser operating at 100 KHz repetition rate with pulse width of 6-8 ps. The target was irradiated with laser powers of 1.5 W and 4.5 W for irradiation times of 10 min and 5 min for the Ag and the Au target, respectively. The laser beam was focused to a spot of about 80 μm in diameter on the surface of the target with a galvanometric scanner. The target surface was scanned on a 10 × 10 mm² area with a scan speed of 800 mm/s. In Fig. 1 we show the scheme of the ps-pulsed laser ablation setup and a detail of the raster-scan pattern made during the ablation process. We carried out profilometry measurements with a stylus scanning method (10 μm lateral resolution; 10 Å vertical resolution).

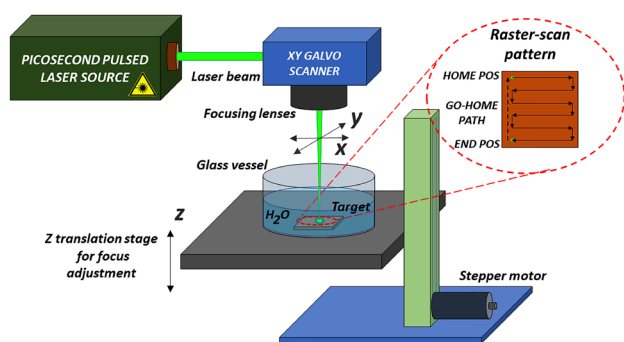


Fig.1: Schematic of picosecond pulsed laser ablation setup.

The optical absorbance spectra of produced colloids were acquired by means of a Perkin–Elmer Lambda 750 UV–vis spectrometer in the 190-900 nm range, using quartz cuvettes. By ultrasonic spraying we deposited a fraction of the colloids on nickel grids to carry out Scanning Transmission Electron Microscopy (STEM) characterization. Another fraction of the colloids was sprayed on glass or on silicon substrates. On the resulting films we carried out optical absorbance and SERS measurements, respectively. STEM images were taken by a scanning electron microscope (ZEISS; model Merlin Gemini 2) operating at an accelerating voltage of 30 kV and at a working distance of 4 mm. SEM images of the craters were acquired at an accelerating voltage of 5 kV and a working distance of 5.6 mm.

All SERS spectra were collected by a Jobin Yvon LabRAM HR800 Raman spectrometer equipped with a 785 nm solid-state laser (Laser XTRA, Toptica Photonics), a 600 grooves mm⁻¹ grating and a Peltier-cooled CCD detector. Notch filters for 785 nm were used to suppress the Rayleigh scattering. The laser was focused on the sample through a 50× Olympus objective (NA=0.75). The nominal laser power at the sample was 0.5 mW, over a spot size of about 1 μm, and an exposure time of 30 s (average of 2 accumulations). The spectra

were recorded in the region between 300 and 2000 cm⁻¹, which encompasses the Raman features of the reference analyte we used, namely crystal violet (CV). The SERS activity of the Ag and Au films was checked using a CV solution at the concentration of 8.9×10⁻⁶ M. The CV solution was prepared in deionized water. The substrates were dipped in these solutions for 20 min, then taken out for free drying in air, then the SERS spectra were collected.

3 Results and discussion

Fig. 1 shows representative crater shapes produced by laser ablation of the Ag target in water, with a laser power of 4.5 W for a fixed number of pulses of 500000. SEM images show that ps laser pulses produce on a target, immersed in the liquid medium, craters whose width slightly changes as a function of the scanner objective-target distance *d*.

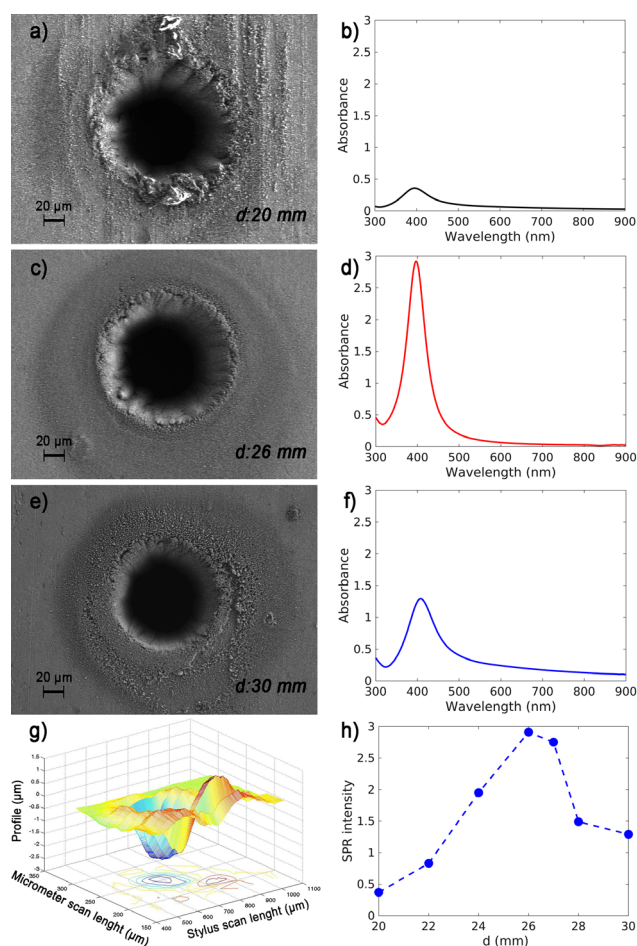


Fig. 2: SEM images of craters produced by ps laser ablation of the Ag target at a laser power of 4.5 W for 500000 pulses (a,c,e), varying the objective-target distance *d*. The optical absorbance spectra of Ag colloids (b,d,f); Crater profile for *d*= 26 mm (g) and effect of objective-target distance *d* on SPR intensity (i.e. on NP productivity) (h). The dashed line is a guide for the eyes.

Moreover, surrounding the edge of the crater, an accumulation of removed material can be envisaged.

This is more evident when the objective-target distance d is fixed at 20 mm and 30 mm, respectively (Fig. 2a,e,g). Otherwise, no ripples and a better defined shape of the crater is found at $d = 26$ mm (see Fig. 2c). For us, this distance represents the optimal focusing condition which, as shown below by optical properties, corresponds to higher ablation efficiency. These observations can be explained taking into account that the removal of mass from the irradiated zone can occur by both thermal and nonthermal mechanisms. The incident laser radiation on the metal creates a large population of highly excited nonequilibrium electrons in a region near the target surface. This electronic excitation can lead to bond breaking of the sample material or “desorption,” and subsequently can cause atomic-size particulate to be ejected from the surface. For a thermal mechanism, the electron energy is redistributed through lattice vibrations and consequently, heat is conducted into the sample. Such heat besides melting the sample can bring its local temperature to the vaporization temperature. Mass removal in the form of micron-sized droplets can also result from hydrodynamic instability of the molten liquid layer. The evaporating vapor can exert a recoil pressure on the melted surface, and molten mass can be pushed radially outward from the irradiated zone [7]. In focusing conditions, the crater has sharp borders and matches the laser spot. This occurs mainly with ultrafast localized laser energy transfer (the machining process occurs via non-linear absorption, enabled by the high intensity in the focus of radiation, resulting in the direct evaporation of the material, in principle, without activating any melting mechanism) when ablation is dominated by direct photoionization processes, thus by locally induced space-charge separation fields and by electron-ion collisions. The crater shape on the target surface is likely to be also affected by the amount of ablated micro/nano particles. This occurs since the laser beam arrives at the target surface after passing through the liquid where a high concentration of micro/nano sized ablated particles is present. In such a condition, a fraction of the laser beam energy gets absorbed by these particles before reaching the target surface, in turn affecting the mass removal efficiency from the irradiated zone [8].

Thus, a first control over the optical properties of Ag and Au NPs must be carried out modulating the beam intensity profile at the target (see Fig. 2g). The colloids, produced with laser power of 4.5 W and irradiation time of 10 min in the three selected focusing conditions show that: (1) the Surface Plasmon Resonance (SPR) peak position remains almost unchanged; (2) its intensity changes as a function of d (see Fig. 2b,d,f). On the overall, it emerges that the higher Ag NP amount was obtained for d value of 26 mm. Similar results were obtained using the Au target (not shown).

The NP productivity of ultra-short pulse laser ablation mainly depends on the pulse energy or fluence and on the pulse repetition rate used in processing. Both these factors are limited by physical processes. The pulse energy is limited by thermal diffusivity in the material, in turn affected by the quality of the processed specimen. For a given pulse energy the ablation rate can be

increased by using a higher average power and a higher frequency. This allows to inject laser energy into the material without using unreasonably high pulse energies. The frequency is restricted by shielding caused by the ejected material, whether in the form of plasma, vapour, liquid or particles. In our case, the laser repetition frequency is not a relevant parameter limiting the NP productivity.

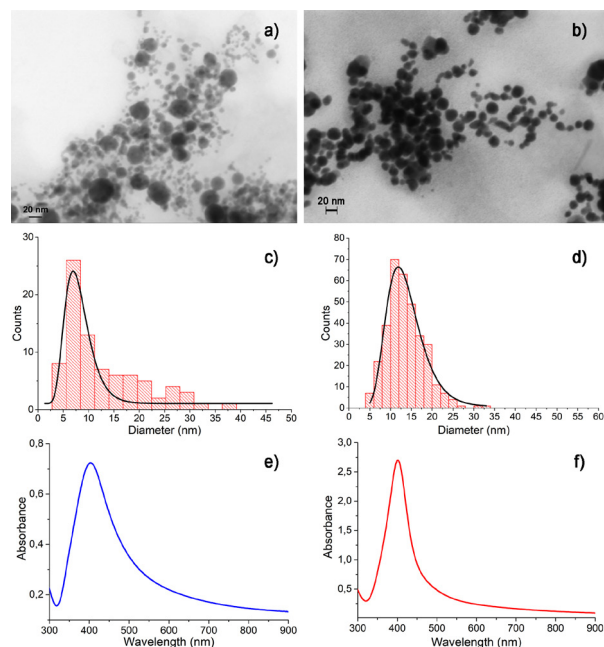


Fig. 3: STEM images, averaged size distribution and optical absorbance spectra of Ag colloids prepared at the laser fluence of 0.5 J/cm^2 (a,c,e) and 1.5 J/cm^2 (b,d,f), respectively.

Keeping fixed the objective-target distance d at 26 mm, for which we found the highest NP productivity, we investigated the effects of the laser fluence on the optical/morphological properties of the colloids. In Fig. 3 are shown STEM images and optical absorbance spectra of Ag colloids prepared at the laser fluence of 0.5 and 1.5 J/cm^2 , respectively. In the sample prepared at 0.5 J/cm^2 , nearly spherical NPs with a diameter of about 8 nm are observed (see Fig. 3c). Few NPs larger than 40 nm are also evident. Increasing the laser fluence (1.5 J/cm^2) the spherical NPs, whose size is of about 15 nm, often agglomerate and overlap (see Fig. 3d). We show in Fig. 3e-f the trend of the UV-Vis absorption spectra as a function of the different morphologies. We observe that the SPR peak intensity increases and the Full Width at Half Maximum (FWHM) decreases, when we increase the laser fluence, keeping fixed all other deposition parameters.

In Fig. 4 are shown a STEM representative image, the size distribution and the optical absorbance spectrum of Au colloids prepared at the laser fluence of 1.5 J/cm^2 . A similar trend was observed for the colloids prepared at 0.5 J/cm^2 (not shown). A high NP productivity as well as a uniform and narrow size distribution (centred around 9 nm) emerges from STEM image analysis. These

evidences are confirmed by the relatively narrow SPR lineshape centred at about 505 nm.

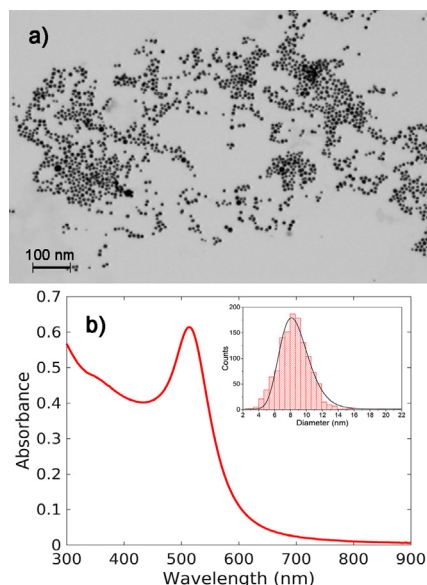


Fig. 4: Representative STEM image (a) and optical absorbance spectrum (b) of Au colloids prepared at the laser fluence of 1.5 J/cm^2 . In the inset of Fig.4b the NP colloid size distribution.

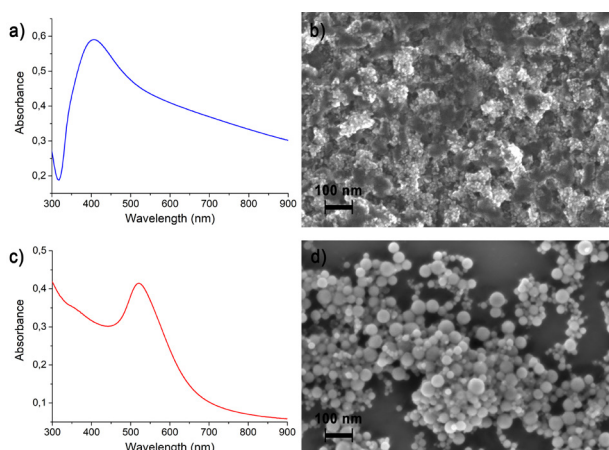


Fig. 5: UV-vis optical absorbance spectra (a,c) and SEM images (b,d) of the films obtained spraying Ag and Au colloids on a Si support (a,b).

Fig. 5a,c show the optical absorbance spectra of the films obtained spraying Ag and Au colloids on glass substrates. A red-shift and a broadening of the width of the SPR peak is observed, mainly for Ag sample. This behavior is ascribed to a clustering process occurring during the transfer of colloids onto the substrates. In fact, different surface morphologies, from isolated nearly spherical NPs, detected by STEM images, to larger

islands (agglomerates) with smooth edges were observed by means of SEM the inhomogeneous films sprayed on the support (see Fig. 5b,d).

We tested the sprayed films for their SERS activity. We report in Fig. 6 preliminary SERS spectra measured from the Ag and Au films on silicon after exposition to an aqueous solution of CV (concentration $8.9 \times 10^{-6} \text{ M}$). For both films we observe well resolved SERS spectra, showing all expected features of CV, *i.e.*, the main peaks located at about 420, 441, 725, 780, 915, 1173, 1392, 1587, 1619 cm^{-1} [9].

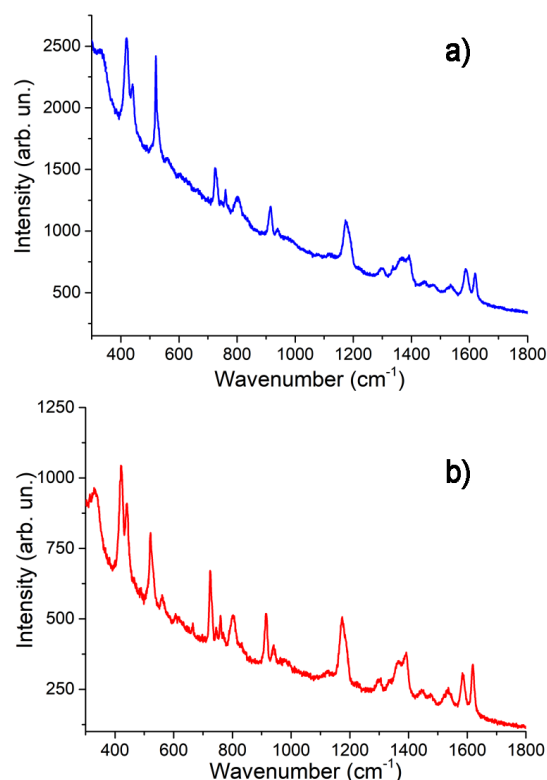


Fig. 6: Raman spectra of crystal violet in H_2O at the concentration $8.9 \times 10^{-6} \text{ M}$ adsorbed onto the surface of the Ag (a) and Au (b) samples, respectively. Exciting line wavelength: 785 nm.

4 Conclusion

In conclusion we used an highly efficient “green” technique based on a laser ablation process to prepare in water Ag and Au nanocolloids. Ag and Au NPs as active SERS substrates were successfully synthesized by a simple spraying procedure of the obtained colloids onto inert supports. The promising SERS action of the Au and Ag nanostructured films, that was checked against CV as the probe molecule using an excitation at 785 nm, is due to suitable plasmon characteristics induced by NP clustering.

References

- 1 V. Amendola, M. Meneghetti, Phys. Chem. Chem. Phys., **11**, 3805 (2009).
- 2 G.Lentini, E. Fazio, F. Calabrese, L. M. De Plano, M. Puliaficio, D. Franco, M. S. Nicolò, S. Carnazza,

- S. Trusso, A. Allegra, F. Neri, C. Musolino,, S. P.P. Guglielmino, *Biosensors and Bioelectronics* **74**, 398 (2015).
- 3 N. R. Agarwal, E. Fazio, F. Neri, S. Trusso, C. Castiglioni, A. Lucotti, N. Santo, P.M. Ossi, *Cryst. Res. Technol.* **46**, 836 (2011).
 - 4 S. Petersen, S. Barcikowski, *J. Phys. Chem. C* **113**, 19830 (2009).
 - 5 D. Zhang, B. Gokce, *Appl. Surf. Sci.* **392**, 991 (2017).
 - 6 L. Gamrad, C. Rehbock, J. Krawinkel, B. Tumursukh, A. Heisterkamp, S.Barcikowski, *J. Phys. Chem. C* **118**, 10302 (2014).
 - 7 A. Semerok, C. Chaleard, V. Detalle, J.-L. Lacour, P. Mauchien, P. Meynadier, C. Nouvellon, B. Salle, P. Palianov, M. Perdrix, G. Petite, *Appl. Surf. Sci.* **138**, 311 (1999).
 - 8 V. Amendola, M. Meneghetti, *Phys. Chem. Chem. Phys.* **15**, 3027 (2013).
 - 9 F. A. Harraz, A.A. Ismail, H. Bouzid, S. A. Al-Sayari, A. Al-Hajry, M.S.Al-Assiri, *Appl. Surf. Sci.* **331**,241 (2015).